2nd URSI AT-RASC, Gran Canaria, 28 May – 1 June 2018

A Circuit Model of the Automotive and Military Test Setups for Disturbance E-field Measurement with Rod Antenna

Carlo Carobbi
Department of Information Engineering
University of Florence, Firenze, ITALY

Abstract

A lumped equivalent circuit model of the CISPR 25 Absorber Lined Shielded Enclosure (ALSE), the RE102 MIL-STD 461G test setups and their variants aimed at improving measurement reproducibility is derived. The lumped model permits to quantitatively describe and provide physical insight into the different test setups.

1. Introduction

A lumped equivalent circuit model is here derived for each of the test setup configurations sketched in Fig. 1, Fig. 2, Fig. 3 and Fig. 4 which correspond to the variants, proposed up to now in the standards and in technical and scientific literature, to the automotive and military test setup for E-field disturbance measurements in the frequency range comprised between 10 kHz and 30 MHz [1-2]. The essential elements of the test setup are: the source of disturbance; an elevated ground plane shorted to the shielded enclosure of an anechoic chamber (ground); a rod antenna with its counterpoise; a metallic extension connecting the elevated ground plane to the counterpoise. Fig. 1 corresponds to the Absorber Lined Shielded Enclosure (ALSE) test setup according to the standard CISPR 25 [1]. Fig. 2 corresponds to the test setup RE102 according to MIL-STD 461G [2]. Fig. 3 corresponds to the variant suggested in [3-6] in order to eliminate resonances that severely limit the reproducibility of this test method. Fig. 4 corresponds to the simplified test setup where measurement is performed on a large, non-elevated, ground plane which represents the reference measurement.

Such resonances have already identified in the 80s (see [7-9]) and verified through several round robins and dedicated experimental analysis [10-14].

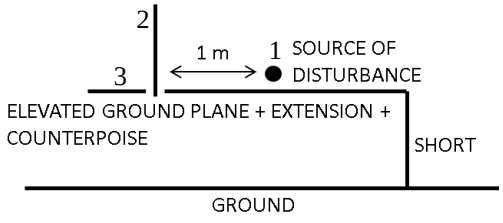

Figure 1. Side view (stylized) of the CISPR 25 ALSE test setup.

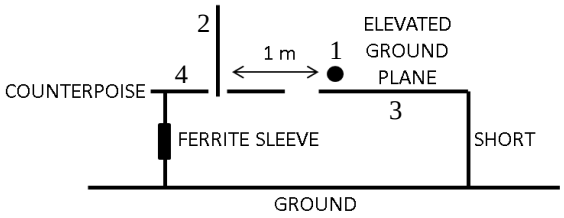

Figure 2. Side view (stylized) of the MIL-STD 461G RE102 test setup.

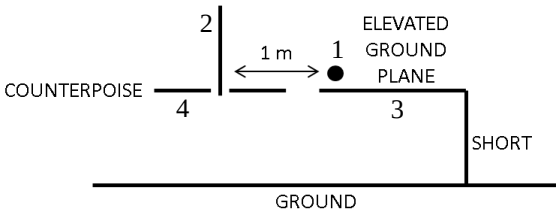

Figure 3. Side view (stylized) of the test setup with floating counterpoise.

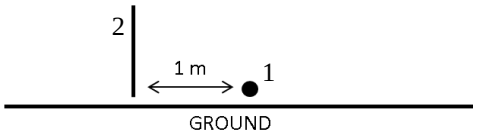

Figure 4. Side view (stylized) of the test setup on the floor.

Commercial software for electromagnetic field simulation (FEKO) is used to the purpose of lumped modelling. The model is capacitive and therefore it is valid up to a few megahertz, i.e. in the frequency range where propagation phenomena are negligible. The model is slightly modified in section 3 in order to take into account the non-ideal ground connection of the elevated counterpoise, inductive effects originated by the setup of propagation phenomena and losses due to absorbers.

The aim of this work is to demonstrate, by using the lumped model, that the test setup corresponding to the configuration in Fig. 3 severely departs from the reference configuration in Fig. 4 in that the E-field level measured adopting the configuration in Fig. 3 is about 20 dB lower than that measured adopting the reference configuration in

Fig. 4. Further the claimed improvement of measurement reproducibility is, by no way, assured.

2. Lumped capacitive model

The following convention for numbering the different elements of the setup is adopted: 1 is the long wire antenna described in Annex J of [1] (the source of the disturbance, in all configurations); 2 is the rod (all configurations); 3 is the elevated ground plane, in the configurations in Fig. 2 and Fig. 3, and the combination of the elevated ground plane, extension and counterpoise in the configuration in Fig. 1; 4 is the counterpoise in the configurations in Fig. 2 and Fig. 3. The following geometrical dimensions have been adopted: The length of the rod is 1 m; The length of the long wire is 0.5 m, suspended at 5 cm above the elevated ground plane and at 10 cm from its front edge; The elevated ground plane has size 1,0 m x 2.5 m; The counterpoise has size 0.6 m x 0.6 m; The extension has size 0.6 m x 0.6 m; The elevation of the elevated ground plane, counterpoise and extension over the ground is 0.9 m. The capacitances C_{ij} are numerically computed at 100 kHz, i.e. at a frequency where propagation effects are negligible. Appropriate loading and feeding conditions [15, Section 4.9] have been implemented at the terminals 1, 2, 3 and 4 in order to determine the various capacitances. The following convention is also adopted: if $i \neq j$ C_{ij} represents the capacitance coupling element i with element j; C_{ii} represents the capacitance of element i to ground. The results of the numerical computation are reported in Tab. 1. Six capacitors are necessary to represent all the possible couplings for the configuration in Fig. 1; Ten capacitors are needed for the configurations in Fig. 2 and Fig. 3 and only three capacitors for the configuration in Fig. 4. The measurement unit of the capacitance is picofarad and all the values are expressed with two significant figures. Note that, due to fringing effect, the capacitance C_{33} for the configuration in Fig. 1 is smaller than the sum $C_{33} + C_{44}$ for the configurations in Fig. 2 and Fig. 3.

Table 1. Capacitances of the equivalent lumped model. All values are in picofarad and expressed with two significant figures.

C_{11}	C_{12}	C_{13}	C_{14}	C_{22}	C_{33}	C_{44}	C_{23}	C_{34}	C_{24}
Fig. 1									
0.22	0.017	6.7	---	4.6	93	---	5.9	---	---
Fig. 2 and Fig. 3									
0.36	0.024	6.7	0.097	4.9	91	23	1.3	5.0	4.3
Fig. 4									
7.5	0.015	---	---	11	---	---	---	---	---

The lumped equivalent circuit model for the configuration in Fig. 1 is shown in Fig. 5. Resistor R represents the input resistance of the matching unit. The value $R = 1$ MΩ has been chosen. R is negligible above 15 kHz due to the relatively large capacitance in parallel $C_{22} + C_{23} = 10.5$ pF. Note also that C_{33} is short-circuited. V_1 and R_1 represent the Thévenin equivalent of the voltage source feeding the long wire antenna and its 50 Ω load. The voltage V_1 is 110 dB(μV) (0.316 V), as required for ALSE validation in Annex J of [2]. Hence the electric field is simply given by the voltage across terminals 2 and 3, V_{23}, times the antenna factor of the rod antenna which is 2/m.

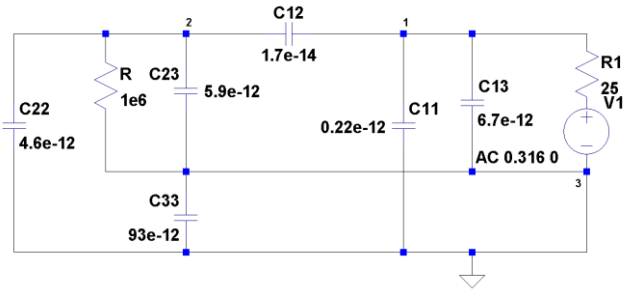

Figure 5. Lumped equivalent circuit model for the configuration in Fig. 1.

It turns out that $V_{23} = 505$ μV at 100 kHz and therefore the electric field is 1010 μV/m, or 60.1 dB(μV/m) that fairly matches the low-frequency value in Table J.1 of [1]. Approximately the same value is obtained in the configuration in Fig. 4. The corresponding equivalent circuit model is represented in Fig. 6.

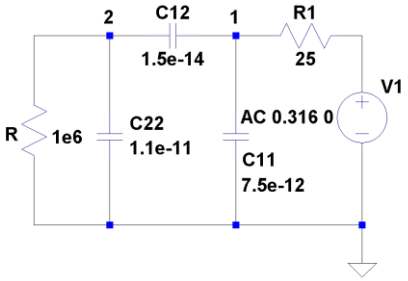

Figure 6. Lumped equivalent circuit model for the configuration in Fig. 4.

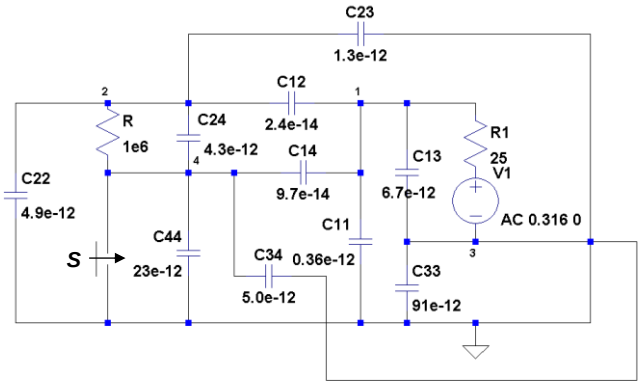

Figure 7: Lumped equivalent circuit model for the configuration in Fig. 2 and Fig. 3 if the switch S is closed and opened, respectively.

The voltage developed between terminal 2 and ground is $V_2 = 430$ μV which corresponds to 860 μV/m, i.e. 59 dB(μV/m). Also this value is pretty well confirmed by those reported in Table J.1 of [1]. We now consider the lumped equivalent circuit model corresponding to the configurations in Fig. 2 and Fig. 3, i.e. the one shown in

Fig. 7. The circuit model is a bit more complicated than the previous ones. If switch S is closed we have the configuration in Fig. 2, otherwise we have the one in Fig. 3. The voltage across terminals 2 and 4, V_{24}, is the one across rod antenna terminals.

It is now interesting to observe that if S is open (floating counterpoise) then, since node 3 is grounded, C_{33} is short-circuited, C_{13} is in parallel with C_{11}, C_{44} is in parallel with C_{34} and C_{22} is in parallel with C_{23}. The result is that nodes 2 and 4 are the extremes of the diagonal of a bridge circuit whose vertexes are nodes 1, 2, 4 and ground, see Fig. 8.

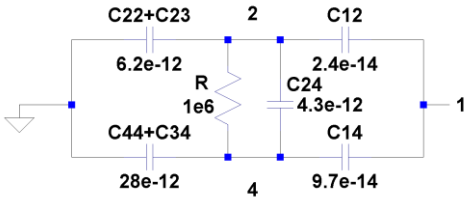

Figure 8. Nodes 2 and 4 in Fig. 7 are the extremes of the diagonal of a bridge circuit whose vertexes are nodes 1, 2, 4 and ground.

In addition we have that $C_{12} = 0.024$ pF, $C_{14} = 0.097$ pF, $C_{22} + C_{23} = 6.2$ pF, $C_{44} + C_{34} = 28$ pF, and

$$\frac{C_{12}}{C_{14}} \cdot \frac{C_{44}+C_{34}}{C_{22}+C_{23}} = 1.1 \qquad (1)$$

Hence the bridge circuit is quite close to equilibrium and therefore the voltage across the rod terminals is close to zero. Indeed at 100 kHz $V_{24} = 68$ μV and the electric field is 136 μV/m, i.e. 43 dB(μV/m). If S is closed (counterpoise grounded) then one side of the bridge circuit (that between nodes 2 and 4) is short-circuited, $V_{24} = 710$ μV and the electric field is 1420 μV/m or 63 dB(μV/m), i.e. 20 dB more. It is now important to observe that since in the floating configuration the measured voltage is the one across the diagonal of a nearly balanced bridge circuit then a small change of the values of the capacitances on the sides of the bridge can produce a large effect on the measured voltage. If for example a metallic box is added below and in contact with the counterpoise having size 20 cm x 20 cm x 40 cm then, in the floating configuration, the measured electric field increases by 4 dB, while it is not varied in the grounded configuration.

3. Extending the frequency range of validity of the lumped model

It is wishful thinking that a lumped equivalent circuit model of the automotive or military test setup may precisely predict the measured electric field up to 30 MHz. It has indeed been demonstrated that propagation phenomena are not negligible beyond few megahertz [7-10] and the complex effect of the absorbers plays an important role, which is peculiar to the setup realized in a given test facility [13, 14]. It is however interesting and instructive to observe that the typical signature of the measured electric field and the order of magnitude are reproduced by replacing the ideal short-circuit of the elevated ground plane to ground with a resistor R_3 in series with an inductor L_3, see Fig. 9.

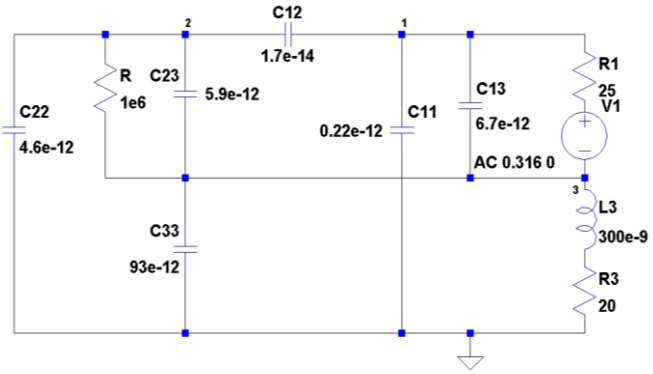

Figure 9. The same lumped model as the one in Fig. 5 but including resistor R_3 and inductance L_3 that account for imperfect ground connection of the elevated counterpoise and propagation.

The resistor is associated with the losses due to the absorbing material, while the inductor reflects the imperfect ground connection of the elevated ground plane and the setup of propagation phenomena at high frequency. The values $L_3 = 300$ nH and $R_3 = 20$ Ω result from an educated guess rather than from a precise calculation based on a physical model but, as we see now, this is acceptable.

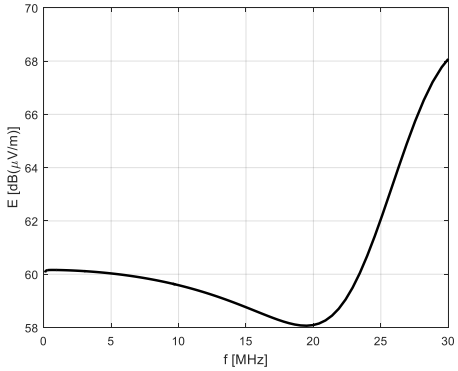

Figure 10. Electric field calculated through the use of the lumped model in Fig. 13.

The result of the computation of the electric field based on the lumped model in Fig. 9 is shown in Fig. 10, which reproduces the signature of the plots in the figures at pages 40, 41 and 42 of [12].

It is evident the negative role of C_{11} and C_{22} that drain an unwanted current to ground. Hence a further improvement of the automotive test setup (in addition to those already listed in [11, 12]) is to increase the size of the counterpoise and the extension to the elevated ground plane in order to reduce C_{11} and C_{22} (and increase C_{23}). This is shown in Fig. 11. This countermeasure demonstrated to be effective in improving the ALSE performance reducing the deviation of the measured

electric field from the reference values in Table J.1 of [1] to within the required 6 dB tolerance.

Figure 11. Increasing the size of the counterpoise and extension in order to reduce the unwanted displacement current to ground through C_{11} and C_{22} (see Fig. 7).

Another interesting consideration that arises from the analysis of the equivalent circuit in Fig. 9 is that, at high-frequency, the voltage to ground of the counterpoise, V_3, is greater than the voltage that should be detected by the matching unit, V_{23}. This is illustrated in Fig. 12, where the ratio $|V_{23}/V_3|$ (in decibel) is shown as a function of frequency. It is seen that above 10 MHz $|V_3|$ is comparable or even greater than $|V_{23}|$, hence an adequate (e.g. 20 dB up to 30 MHz) common mode rejection is required for the matching unit in order to correctly detect $|V_{23}|$.

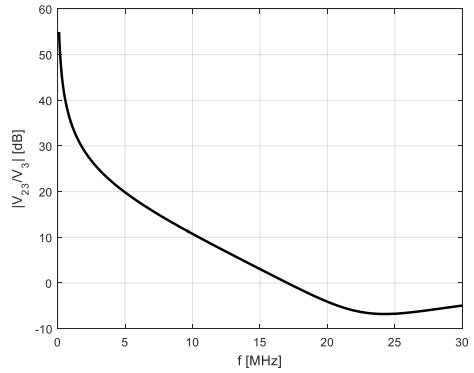

Figure 12. Ratio, in decibel, between the magnitude of the voltages V_{23} and V_3, as a function of frequency.

7. References

1. Vehicles, boats and internal combustion engines - Radio disturbance characteristics - Limits and methods of measurement for the protection of on-board receivers, CISPR 25, 4th ed., 2016.

2. Department of defense interface standard requirements for the control of electromagnetic interference characteristics of subsystems and equipment, MIL STD 461G, US Dept. of Defense, Dec. 2015.

3. K. Javor, "On the nature and use of the 1.04 m electric field probe," Interference Technology, 2011, pp. 66-77.

4. H. W. Gaul, "Electromagnetic Modeling and Measurements of the 104 cm Rod and Biconical Antenna for Radiated Emissions Testing Below 30 MHz," IEEE International Symp. on EMC, 2013, pp. 434-438.

5. K. Javor, "MIL-STD-461G: The 'Compleat' Review," Interference Technology Engineering Master (ITEM), April 2016.

6. A. Gandolfo, R. Azaro and D. Festa, "Improving the Accuracy of Radiated Emission Measurements for Frequency Below 30 MHz by using a Fiber Optic Isolated Rod Antenna," 2017 IEEE Int. Symp. on EMC, Washington (DC), Aug. 2017, pp. 63-68.

7. A. C. Marvin, "The use of screened (shielded) rooms for the identification of radiation mechanisms and the measurement of free-space emissions from electrically small sources", IEEE Trans. Electromag. Compat., vol. 26, no. 4, Nov. 1984, pp. 149-153.

8. A. C. Marvin, L. Steele, "Improved techniques for the measurement of radiated emissions inside a screened room," IEE Electronics Letters, vol. 22, no. 2, Jan. 1986, pp. 94-96.

9. L. Dawson, A. C. Marvin, "New screened room techniques for the measurement of RFI," Journal IERE, vol. 58, no. 1, Jan/Feb 1988, pp. 28-32.

10. Turnbull, L., "The Groundplane Resonance – Problems with Radiated Emissions Measurements Below 30 MHz", Automotive EMC Conference 2007, Newbury, UK, 16th Oct 2007, pp. 1-13.

11. C. Carobbi and D. Izzo, "Reproducibility of CISPR 25 ALSE Test Method," 2017 IEEE Int. Symp. on EMC, Washington (DC), Aug. 2017, pp. 57-62.

12. C. Carobbi, "Issues in E-field measurements between 10 kHz and 30 MHz," 2017 IEEE Int. Symp. on EMC, Washington (DC), Aug. 2017, DOI: 10.1109/ISEMC.2017.8078024.

13. F. Lafon, R. Dupendant and J. Davalan, "Invesigation on dispersions between CISPR25 chambers for radiated emissions below 100 MHz," EMC Europe, 2014, pp. 29-34.

14. F. Lafon, J. Davalan and R. Dupendant, "Inter-laboratory Comparison Between CISPR 25 Chambers, Identification of Influent Parameters and Analysis by 3D Simulation," APEMC, 2015, pp. 71-74.

15. S. Ramo, J. R. Whinnery and T. Van Duzer, Fields and Waves in Communication Electronics, John Wiley and Sons, Inc., 3rd ed., New York, 1994.